Soft Matter

COMMUNICATION

View Article Online
View Journal | View Issue

Cite this: *Soft Matter*, 2020, **16**, 4350

Received 13th January 2020,
Accepted 16th March 2020

DOI: 10.1039/d0sm00078g

rsc.li/soft-matter-journal

Role of molecular bend angle and biaxiality in the stabilization of the twist-bend nematic phase†

Wojciech Tomczyk * and Lech Longa *

What are the prerequisites for acquiring a stable twist-bend nematic phase (N_{TB})? Addressing this question has led to the synthesis of a vast number of new compounds, concluding each time that the molecule's shape is one of the predominant factors. Inspired by the expanding knowledge of different achiral bent-shaped molecules forming a twist-bend nematic phase, we reinvestigate the interplay between a molecule's bend angle and a molecule's arms molecular biaxiality. Employing our previously developed generalized mean-field model, we explore more obtuse bend angles. We observe direct phase transition sequences between locally biaxial and uniaxial variants of N_{TB}, along with biaxial and uniaxial nematic phases. Additionally, we present a comprehensive overview of how phase diagrams evolve according to alterations in the value of the bend angle and the magnitude of biaxiality.

Twist-bend nematic (N_{TB}) is a one dimensional modulated phase, which forms through spontaneous chiral symmetry breaking in the isotropic and nematic phases of liquid crystalline systems. As it contradicted common knowledge, the discovery of N_{TB} engulfed the interest of the worldwide liquid crystal community.[1] In N_{TB}, the nematic director $\hat{\mathbf{n}}$ is spontaneously distorted:

$$\hat{\mathbf{n}}(z) = [-\sin(\theta)\sin(\phi),\sin(\theta)\cos(\phi),\cos(\theta)], \qquad (1)$$

where θ is the conical angle, and $\phi = kz = 2\pi z/p$ is the azimuthal angle associated with the wavevector $\mathbf{k} = k\hat{\mathbf{z}}(k = \pm 2\pi/p)$ and period p. This distortion leads to the formation of a conical helix (like in the smectic C^*, but without long-range positional order of molecules) with a nanoscale period. The $\pm$ sign indicates the degeneracy in the handedness of chiral domains (either left- or right-handed), called ambidextrous chirality.

Conclusions drawn from the theoretical foundations provided by Meyer[2] and Dozov[3] regarding the influence of flexopolarization and conditions imposed on elastic constants indicated that the emergence of N_{TB} can be facilitated by the structure of a properly "bent" molecule. Thus, the first compound that exhibited long sought-after N_{TB} was a dimer, 4′,4′-(heptane-1,7-diyl)bis([1′,1″-biphenyl]-4″-carbonitrile) (abbreviated as CB7CB[4–6]), where two 4-cyanobiphenyls (CB) are linked by an alkylene spacer (C_7H_{14}). CB7CB is a member of the 1,ω-bis(4-cyanobiphenyl-4′-yl) alkane homologous series, which is denoted by the acronym CB*n*CB, where n refers to the number of methylene units in the flexible spacer. Within this series, only molecules with an odd number of methylene units in the spacer are able to form N_{TB}.[7]

Further, structure-focused,[8–13] research solidified the molecular curvature as one of the profound driving forces in the stabilization of N_{TB}. Even a small change in molecular structure, like taking CB7CB and substituting each of the methylene units linked with the 4-cyanobiphenyls by oxygen or sulfur,[14] can result in a substantial modification of the molecule's average bend. Since the discovery of N_{TB}, the "family of compounds" capable of forming this phase has been expanded, *i.e.* by hybrid bent-core LC trimers,[15] hydrogen-bonded oligomers,[16] a duplexed hexamer,[17] trimers, oligomers and polymers.[18–20] Moreover, due to the tremendous interest in resolving the ambiguities linked to the structural features of N_{TB}, new phases have been discovered: twist-bend smectic C (SmC_{TB})[21] and twist-grain-boundary-twist-bend (TGB_{TB}).[22]

Inspired by continuing advances in the synthesis of new N_{TB}-forming compounds with different degrees of molecule's core bent,[14,23–26] we reinvestigate our generalized mean-field model[27] for V-shaped molecules.

We start our considerations by recalling the assumptions of the model. Molecular reference frames are constructed out of two mesogenic arms, A and B, each of length L, arranged reciprocally at an angle χ (Fig. 1). It is assumed that the precession of $\hat{\mathbf{n}}(z)$ is followed by two other directors:

$$\hat{\mathbf{m}}(z) = [\cos(\phi),\sin(\phi),0], \qquad (2)$$

$$\hat{\mathbf{l}}(z) \equiv \hat{\mathbf{n}}(z) \times \hat{\mathbf{m}}(z) = [-\cos(\theta)\sin(\phi),\cos(\theta)\cos(\phi),-\sin(\theta)]. \qquad (3)$$

This parametrization (eqn (1)–(3)) permits the N_{TB} phase for $0^\circ < \theta < 90^\circ$ and finite pitch p, with wave vector $\mathbf{k}$ being parallel to the $\hat{\mathbf{z}}$ axis.

Institute of Theoretical Physics, Jagiellonian University, Łojasiewicza 11, 30-348 Kraków, Poland. E-mail: wojciech.tomczyk@doctoral.uj.edu.pl, lech.longa@uj.edu.pl

† Electronic supplementary information (ESI) available. See DOI: 10.1039/d0sm00078g

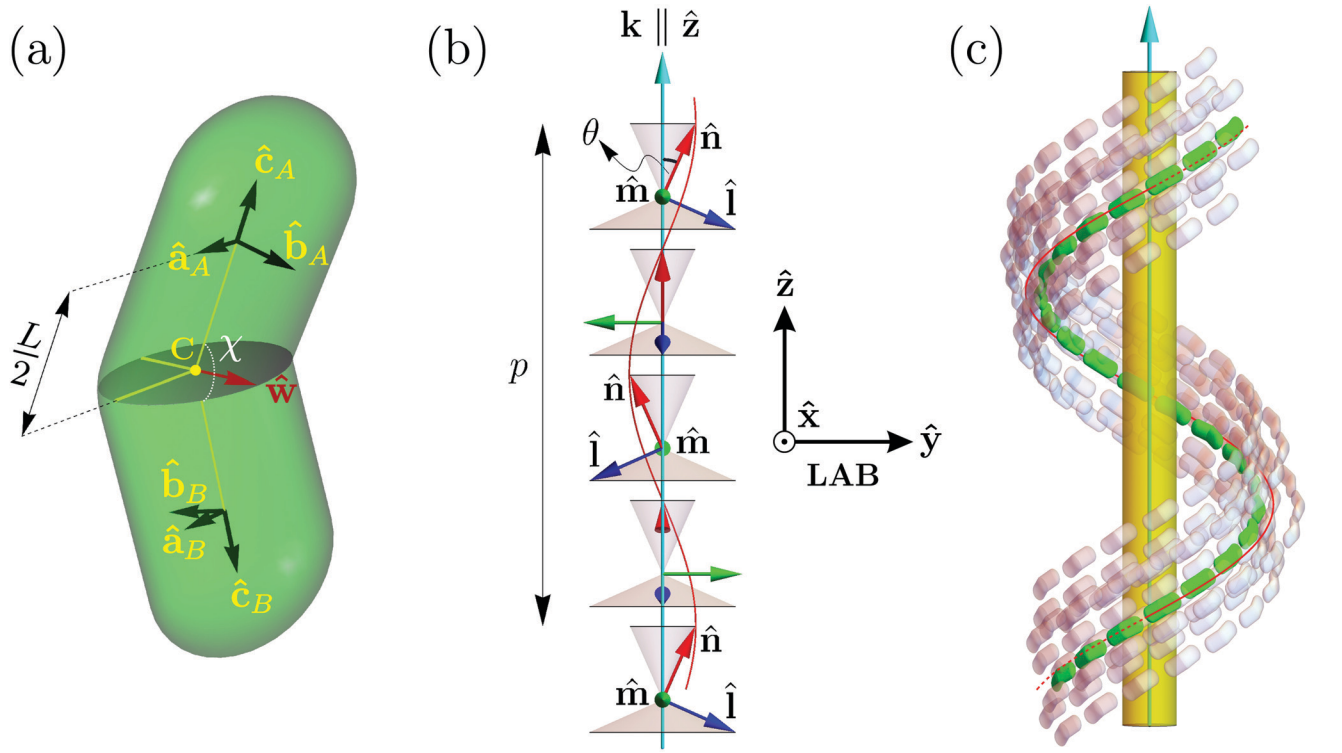

Fig. 1 (a) Features of the bent-shaped molecule adopted within our generalized mean-field model. The lengths of the arms L are taken to be equal. The mutual positioning of the arms is implied by the bend angle χ. The molecular basis for arm A is given by an orthonormal tripod of vectors $\Omega_A = \{\hat{\mathbf{a}}_A,\hat{\mathbf{b}}_A,\hat{\mathbf{c}}_A\}$, and by $\Omega_B = \{\hat{\mathbf{a}}_B,\hat{\mathbf{b}}_B,\hat{\mathbf{c}}_B\}$ for arm B. The molecule's C_2 (molecular) symmetry axis coincides with the unit vector $\hat{\mathbf{w}}$ attached at point C. Figure reproduced from ref. 27 with permission from the Royal Society of Chemistry. (b) Visualization of the local directors used in the mean-field ansatz for the N_{TB} structure, where the local director basis $\{\hat{\mathbf{n}},\hat{\mathbf{m}},\hat{\mathbf{l}}\}$ on each arm undergoes a heliconical precession around an axis $\hat{\mathbf{z}}$ ($\phi = kz = (2\pi/p)z$). This structure is characterized by the finite period p, which can also be expressed *via* wavevector $\mathbf{k}$ ($\mathbf{k} = k\hat{\mathbf{z}} = \pm(2\pi/p)\hat{\mathbf{z}}$) and heliconical tilt angle θ between the primary director $\hat{\mathbf{n}}$ and the $\mathbf{k}$ axis. (c) Due to the ambidextrous chirality, the N_{TB} helix can be either left- or right-handed. This figure is a schematic depiction of the molecular arrangement in the right-handed N_{TB} phase.

Going forward, the molecular basis is placed at the midpoint of each arm, which will be reflecting the arm's molecular biaxiality. The arms are expressed in terms of a molecular (symmetric and traceless) quadrupolar tensor $\mathbf{Q}$, which is composed of uniaxial ($\mathbf{Q}_U$) and biaxial ($\mathbf{Q}_B$) parts of $D_{\infty h}$ and D_{2h} symmetry, respectively. The expression reads:

$$\mathbf{Q}(\Omega_i) \overset{\text{def}}{=} \mathbf{Q}_U(\hat{\mathbf{c}}_i) + \lambda\sqrt{2}\mathbf{Q}_B(\hat{\mathbf{a}}_i,\hat{\mathbf{b}}_i), \tag{4}$$

where

$$\mathbf{Q}_U(\hat{\mathbf{c}}_i) \overset{\text{def}}{=} \frac{1}{\sqrt{6}}(3\hat{\mathbf{c}}_i \otimes \hat{\mathbf{c}}_i - \mathbb{1}), \tag{5}$$

$$\mathbf{Q}_B(\hat{\mathbf{a}}_i,\hat{\mathbf{b}}_i) \overset{\text{def}}{=} \frac{1}{\sqrt{2}}(\hat{\mathbf{a}}_i \otimes \hat{\mathbf{a}}_i - \hat{\mathbf{b}}_i \otimes \hat{\mathbf{b}}_i), \tag{6}$$

are built out of the right-handed orthonormal tripod $\Omega_i = \{\hat{\mathbf{a}}_i,\hat{\mathbf{b}}_i,\hat{\mathbf{c}}_i\}$ of vectors defining the orientational degrees of freedom of the arm $i = A, B$ (Fig. 1). Parameter λ is a measure of the arm's biaxiality, $\otimes$ denotes the tensor product and $\mathbb{1}$ is the identity matrix.

V-shaped molecules are biaxial due to their C_{2v} symmetry, and this is a shape-originating biaxiality (called λ_{shape}). Thus, for a V-shaped molecule with uniaxial arms, λ_{shape} can be intertwined with molecule's bend angle χ through the formula:[28–30]

$$\lambda_{\text{shape}} = \frac{\sqrt{6}(\cos(\chi)+1)}{2-6\cos(\chi)}. \tag{7}$$

In our model, we let the molecular biaxiality of banana-shaped molecules enter not only through their "V" shape, but also through the biaxiality of molecular arms. This extension allows the arms' molecular biaxiality to be treated as an extra parameter characterizing bent-shaped molecules, in addition to the bend angle.

The last element of the molecule's structure is the unit vector $\hat{\mathbf{w}}$ at the center (C) of the molecule (associated with the molecular C_2 axis, see Fig. 1a), which, combined with $\hat{\mathbf{m}}$ through calculating $\langle\hat{\mathbf{w}}\cdot\hat{\mathbf{m}}(z = R_C)\rangle$, gives an indication of the polar order in the system.

In the next step the director basis is constructed:

$$\bar{\mathbf{Q}}(R_i) = \bar{\mathbf{Q}}_U(R_i) + \bar{\mathbf{Q}}_B(R_i) = q_0\mathbf{Q}_U(\hat{\mathbf{n}}(R_i)) + q_2\mathbf{Q}_B(\hat{\mathbf{m}}(R_i),\hat{\mathbf{l}}(R_i)), \tag{8}$$

wherein $\{\hat{\mathbf{n}}(R_i),\hat{\mathbf{m}}(R_i),\hat{\mathbf{l}}(R_i)\}$ are three local directors at the position R_i of the midpoint of the i-th arm ($i = A, B$), and q_0 and q_2 are the uniaxial and biaxial order parameters of an arm, respectively. The local directors are identified with eigenvectors

of the $\bar{\mathbf{Q}}$ tensor and the corresponding eigenvalues[31] are given by $\mu_m = -q_0/\sqrt{6} + q_2/\sqrt{2}$, $\mu_l = -q_0/\sqrt{6} - q_2/\sqrt{2}$ and $\mu_n = -\mu_m - \mu_l = \sqrt{2/3}q_0$. In this framework the locally isotropic phase is realized when all three eigenvalues of $\bar{\mathbf{Q}}$ are equal ($\bar{\mathbf{Q}} \equiv \mathbf{0}$). On the other hand, when two out of the three eigenvalues of $\bar{\mathbf{Q}}$ are identical, *i.e.* $q_0 \neq 0$, $q_2 = 0$ or $q_0 \neq 0$, $q_2 = \sqrt{3}q_0$ or $q_0 \neq 0$, $q_2 = -\sqrt{3}q_0$, then this is referred to as a locally $D_{\infty h}$-symmetric uniaxial state. Yet the most generic case is described by $\bar{\mathbf{Q}}$ possessing three different real eigenvalues, reflecting the local D_{2h}-symmetric biaxial state. Generally, these properties can be expressed using the inequality:[31,32]

$$\mathrm{Tr}(\bar{\mathbf{Q}}^2)^3 - 6\mathrm{Tr}(\bar{\mathbf{Q}}^3)^2 \geq 0, \tag{9}$$

which can be denoted with one condition, $w^2 \leq 1$, where:

$$-1 \leq w = \sqrt{6}\frac{\mathrm{Tr}(\bar{\mathbf{Q}}^3)}{\mathrm{Tr}(\bar{\mathbf{Q}}^2)^{3/2}} \leq 1. \tag{10}$$

Thus, w is now a scalar measure of how strongly uniaxial/biaxial the local order is. The edges of eqn (10) are represented by oblate ($w = -1$) and prolate ($w = 1$) uniaxial states, whereas the biaxial state is bounded in between ($w^2 < 1$). In addition, if $w = 0$, this is attributed to a state with so-called "maximal biaxiality".[33]

The complete mean-field Hamiltonian and equilibrium free energy per particle are given by:

$$H_{\mathrm{MF}}(\Omega) = -\varepsilon\mathrm{Tr}[\mathbf{Q}(\Omega_A)\cdot\bar{\mathbf{Q}}(\mathrm{R}_A) + \mathbf{Q}(\Omega_B)\cdot\bar{\mathbf{Q}}(\mathrm{R}_B)] = -\varepsilon\Lambda_{\mathrm{MF}}(\Omega), \tag{11}$$

$$f = {q_0}^2 + {q_2}^2 - t^* \ln Z, \tag{12}$$

where ε is the coupling constant, '·' denotes matrix multiplication, and Ω stands for the molecular orientation expressed in terms of Euler angles that define this orientation in a local $\{\hat{\mathbf{n}},\hat{\mathbf{m}},\hat{\mathbf{l}}\}$ frame.

The orientational one-particle partition function Z is given by:

$$Z = \int \exp[-H_{\mathrm{MF}}(\Omega)/(k_{\mathrm{B}}T)]\mathrm{d}\Omega = \int \exp[\Lambda_{\mathrm{MF}}(\Omega)/t^*]\mathrm{d}\Omega, \tag{13}$$

where $t^* \overset{\mathrm{def}}{=} k_{\mathrm{B}}T/\varepsilon$ is the (dimensionless) reduced temperature. Orientational averages of any one-particle quantity $X(\Omega)$ are calculated in the usual manner as:

$$\langle X(\Omega)\rangle = \frac{1}{Z}\int X(\Omega)\mathrm{e}^{\Lambda_{\mathrm{MF}}(\Omega)/t^*}\mathrm{d}\Omega. \tag{14}$$

The equilibrium structure can be obtained by taking the parametric form of the alignment tensor $\bar{\mathbf{Q}}$ (eqn (1)–(3) and (8)) and minimizing the free energy, eqn (12), with respect to the order parameters q_0 and q_2 along with the "local environment" parameters θ and k (see ESI†). The order parameters are given consistently by:

$$q_n = \frac{1}{2}\langle q_n(\{\mathrm{R}_A\},\Omega_A) + q_n(\{\mathrm{R}_B\},\Omega_B)\rangle, \quad n = 0, 2, \tag{15}$$

where orientational averaging applies to the symmetry adapted functions given in a basic form:[31,32]

$$q_0(\{\mathrm{R}_i\},\Omega_i) = -\frac{1}{2} + \frac{3}{2}(\hat{\mathbf{n}}(\mathrm{R}_i)\cdot\hat{\mathbf{c}}_i)^2 + \lambda\sqrt{\frac{3}{2}}\left[(\hat{\mathbf{n}}(\mathrm{R}_i)\cdot\hat{\mathbf{a}}_i)^2 - (\hat{\mathbf{n}}(\mathrm{R}_i)\cdot\hat{\mathbf{b}}_i)^2\right], \tag{16}$$

$$q_2(\{\mathrm{R}_i\},\Omega_i) = \frac{\sqrt{3}}{2}\left[\left(\hat{\mathbf{l}}(\mathrm{R}_i)\cdot\hat{\mathbf{c}}_i\right)^2 - (\hat{\mathbf{m}}(\mathrm{R}_i)\cdot\hat{\mathbf{c}}_i)^2\right] + \lambda\sqrt{2}\left[\left(\hat{\mathbf{l}}(\mathrm{R}_i)\cdot\hat{\mathbf{a}}_i\right)^2 + (\hat{\mathbf{m}}(\mathrm{R}_i)\cdot\hat{\mathbf{b}}_i)^2 - \frac{1}{2}(\hat{\mathbf{n}}(\mathrm{R}_i)\cdot\hat{\mathbf{c}}_i)^2 - \frac{1}{2}\right], \tag{17}$$

and where the symbol $\{\mathrm{R}_i\} \overset{\mathrm{def}}{=} \{\hat{\mathbf{n}}(\mathrm{R}_i), \hat{\mathbf{m}}(\mathrm{R}_i), \hat{\mathbf{l}}(\mathrm{R}_i)\}$ stands for the right-handed tripod of directors ($i = A, B$).

For additional quantitative information about phases, we also calculate the mean values of the uniaxial ($\langle q_0^k\rangle$) and biaxial ($\langle q_2^k\rangle$) order parameters with respect to the modulation axis $\mathbf{k}\|\hat{\mathbf{z}}$ ($\hat{\mathbf{k}} = \mathbf{k}/\mathrm{k}$) of reference frame $\{\mathrm{R}_{\hat{\mathbf{k}}}\} \overset{\mathrm{def}}{=} \left\{\hat{\mathbf{k}}, \hat{\mathbf{m}}(z = \mathrm{R}_{\mathrm{C}}), \hat{\mathbf{k}} \times \hat{\mathbf{m}}(z = \mathrm{R}_{\mathrm{C}})\right\}$:

$$\langle q_n^k\rangle = \frac{1}{2}\langle q_n(\{\mathrm{R}_{\hat{\mathbf{k}}}\},\Omega_A) + q_n(\{\mathrm{R}_{\hat{\mathbf{k}}}\},\Omega_B)\rangle, \quad n = 0, 2. \tag{18}$$

For non-tilted phases ($\theta = 0$) the following relation holds:[34–36]

$$\langle q_n^k\rangle = q_n \quad n = 0, 2, \tag{19}$$

whereas for tilted phases ($\theta \neq 0$) there will be discrepancies between the order parameters calculated in various reference frames. It means that locally, in the arm reference frames q_2 is zero in the $\mathrm{N_{TB}}$ phase, while in the $\hat{\mathbf{k}}$-frame $\langle q_2^k\rangle$ is non-zero.

The notation for the phases used within the framework of this communication is presented in Table 1.

Fig. 2a shows the phase diagram in the $\{\lambda,t^*\}$ plane for the case where $\chi = 150^\circ$. In this scenario, nematic phases excel over twist-bend nematics through the whole range of λ. Fig. 2b is a magnification of a particularly narrow region of Fig. 2a (bounded by red rectangle), where straight phase transitions occur between all the nematic phases anticipated by the model: $\mathrm{N_U} \leftrightarrow \mathrm{N_B} \leftrightarrow \mathrm{N_{TB}} \leftrightarrow \mathrm{N_{TB,B}}$. Details of the nature of the sequence are shown in Fig. 3. The subsequent transitions $\mathrm{N_B} \leftrightarrow \mathrm{N_{TB}} \leftrightarrow \mathrm{N_{TB,B}}$ are first order with visible discontinuity

Table 1 Five phases described within the generalized mean-field model

Symbol	Description
$\mathrm{N_{TB}}$	Twist-bend nematic phase with a heliconical uniaxial ansatz ($\bar{\mathbf{Q}}_{\mathrm{U}}$)
$\mathrm{N_{TB,B}}$	Twist-bend nematic phase with a heliconical biaxial ansatz ($\bar{\mathbf{Q}}_{\mathrm{B}}$)
$\mathrm{N_U}$	Uniaxial nematic
$\mathrm{N_B}$	Biaxial nematic
I	Isotropic phase

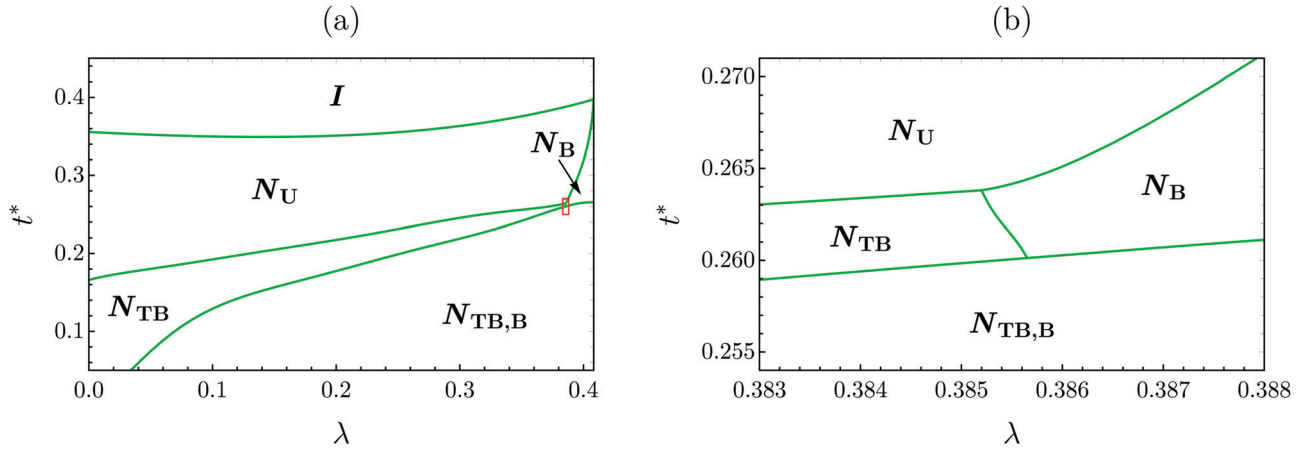

Fig. 2 (a) Phase diagram in the $\{\lambda,t^*\}$ plane for bend angle χ equal to 150°. (b) Magnification of area bounded by red rectangle on panel (a) where $N_U \leftrightarrow N_B \leftrightarrow N_{TB} \leftrightarrow N_{TB,B}$ phase transitions occur.

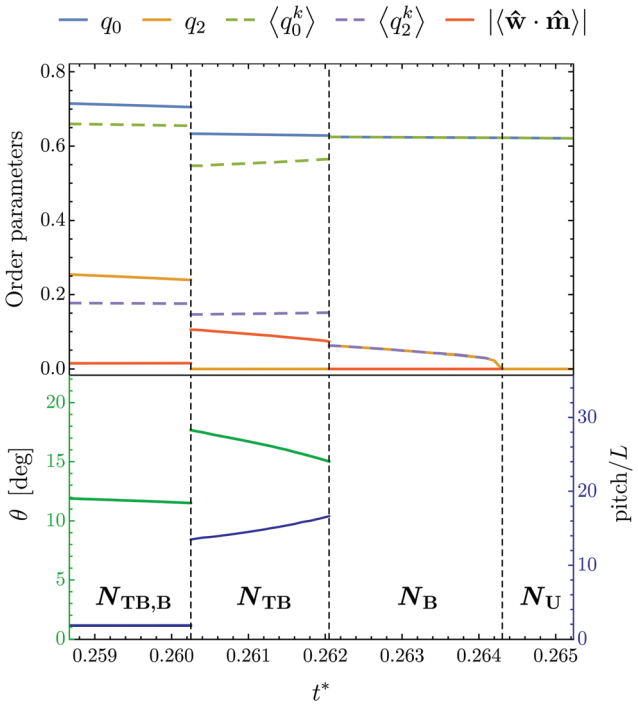

Fig. 3 Behavior of order parameters, tilt angle and pitch for the sequence of phase transitions: $N_U \leftrightarrow N_B \leftrightarrow N_{TB} \leftrightarrow N_{TB,B}$, when $\lambda = 0.3854$ and $\chi = 150°$. Parameters q_0, q_2, θ and k are obtained by the direct minimization of the free energy (eqn (12)); $\langle q_0^k \rangle$ and $\langle q_2^k \rangle$ are uniaxial and biaxial order parameters calculated with respect to the wave vector $\mathbf{k}$, and $|\langle \hat{\mathbf{w}} \cdot \hat{\mathbf{m}} \rangle| \stackrel{\text{def}}{=} |\langle \hat{\mathbf{w}} \cdot \hat{\mathbf{m}}(z = R_C) \rangle|$ is the modulus of the polar order parameter.

in the order parameters, whereas $N_U \leftrightarrow N_B$ is a second order phase transition. The attributes of the $N_B \leftrightarrow N_{TB} \leftrightarrow N_{TB,B}$ transitions are similar to those shown in Fig. 5 of ref. 27 for λ = 0.36 and $\chi = 140°$. Both the tilt angle θ and the pitch are weakly temperature-dependent in $N_{TB,B}$, as opposed to N_{TB}, where the aforementioned parameters strongly depend on the temperature up to the transition to the nematic phase. Additionally, there is a large jump in θ and pitch at the verge of the $N_{TB} \leftrightarrow N_{TB,B}$ phase transition. In the limit $t^* \to 0$ it has been shown[27] that θ obeys the relation:

$$\theta(t^* = 0) = \frac{1}{2}(180° - \chi), \tag{20}$$

which for $\chi = 150°$ yields $\theta = 15°$.

Incrementally increasing the bend angle up to 160° paves the way for the even more dominant presence of nematic phases (Fig. 4a). Shrinkage of the N_{TB} stability range exposes the $N_{TB,B}$ region, which can be reached directly from N_U (Fig. 4b). Hence the phase sequence: $I \leftrightarrow N_U \leftrightarrow N_{TB,B}$, which is a first order phase transition with visible discontinuity in the order parameters (Fig. 5), exhausts the pool of all possible phase transitions within this model.[27] One can see that there is a lesser discrepancy between the local set q_0 and that measured with respect to the modulation axis ($\langle q_0^k \rangle$), and the polar order is feebler compared to the scenario with $\chi = 150°$. According to eqn (20), the limiting value of θ for $\chi = 160°$ is 10° (Fig. 5).

For a comprehensive overview, we also investigated how the λ parameter reshapes the "landscape" of respective phase diagrams in the $\{\chi,t^*\}$ plane. We have intentionally focused on χ from 90° to 180°, as all N_{TB}-forming molecules reported to date possess a bend angle which falls within that range. Furthermore, we have chosen a reference set of points lying on the line $\{\chi,t^* = 0.22\}$ (purple points in Fig. 6a–e) in order to analyze the impact of λ on the behavior of tilt angle, pitch and $w(\bar{\mathbf{Q}}(R_A)) \equiv w(\bar{\mathbf{Q}}_A)$ and compare between the phase diagrams.

The data presented in Fig. 6a significantly broadens the results of Greco *et al.*[37] and T. T. To *et al.*[38] (both are depicted in Fig. 2 herein[38]), which were carried out with a uniaxial approach ($\lambda = 0$). Here, all occurring nematic phases are locally uniaxial (N_U^+, prolate) and N_{TB} is visibly predominant over the range of N_U^- (oblate) and N_B. Direct $I \leftrightarrow N_{TB}$ occurs for $\chi \in [90°,132°]$ and $I \leftrightarrow N_U$ for $\chi = 180°$, whereas for $\chi \in (132°,180°)$ the following phase sequence occurs: $I \leftrightarrow N_U \leftrightarrow N_{TB}$. The tilt angle decreases approximately linearly with the increasing bend angle, in contrast to the pitch, which increases with the augmentation of the bend angle up to the phase transition to N_U.

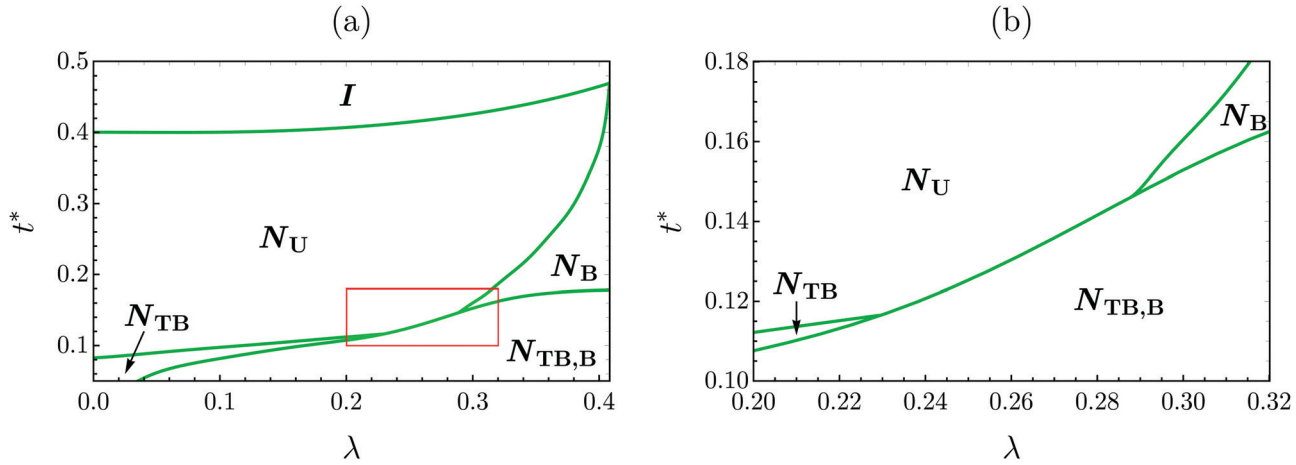

Fig. 4 (a) Phase diagram in the $\{\lambda,t^*\}$ plane for bend angle χ equal to 160°. (b) Magnification of area bounded by red rectanlge on panel (a) where $N_U \leftrightarrow N_{TB,B}$ phase transition occurs.

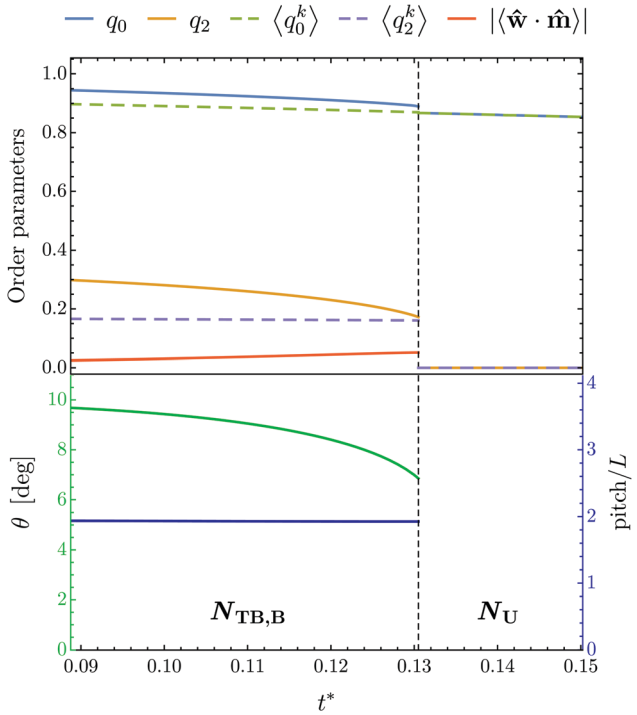

Fig. 5 Behavior of order parameters, tilt angle and pitch for the phase transition: $N_U \leftrightarrow N_{TB,B}$, when $\lambda = 0.26$ and $\chi = 160°$. For further details see the caption for Fig. 3.

Both $I \leftrightarrow N_U$ and $I \leftrightarrow N_U \leftrightarrow N_{TB}$ are frequently observed,[1,39] while straightforward phase transition from isotropic to N_{TB} has been found for only a few compounds[40,41] and mixtures.[42] Fig. 6a supports the conclusions drawn in ref. 38 that N_{TB} might be blocking the formation of N_B for $\lambda = 0$. On the other hand, the inclusion of $\lambda \neq 0$ rearranges the positions in competition between N_B and N_{TB}.

Fig. 6b–e illustrate how the magnitude of biaxiality reshapes the phase diagrams in the domain of $\{\chi,t^*\}$. A common feature of all the presented phase diagrams (Fig. 6a–e) is direct accessibility of a twist-bend nematic (either N_{TB} or $N_{TB,B}$) from the isotropic phase within the spectrum of χ in the interval between 90° and 132° ($\lambda = 0$), and from 90° to 139° ($\lambda = 1/\sqrt{6}$). The boundary case, *i.e.* $\chi = 180°$, reflects the results of the previously studied Maier–Saupe model for biaxial rod-like molecules.[43,44] Increasing λ (Fig. 6b) by small increments of 0.1 wholly reorganizes the previous phase arrangement. Lower temperature N_{TB} is substituted by $N_{TB,B}$ and shifted towards higher temperatures. In an analogous scheme applied to N_U, N_B emerged at lower temperatures, modifying the regime of stability for N_U. For χ from 90° to 118° only a $I \leftrightarrow N_{TB,B}$ phase transition is present. For $\chi \in (118°,136°]$, the aforementioned sequence is separated by N_{TB}, leading to $I \leftrightarrow N_{TB} \leftrightarrow N_{TB,B}$. Changing χ within the range of 136° to 169° introduces an additional phase, namely N_U, between I and N_{TB}. Within a narrow span of $\chi \in (169°,172°]$, the area of N_{TB} vanishes in favor of the $I \leftrightarrow N_U \leftrightarrow N_{TB,B}$ sequence. However, for $\chi \in (172°,180°)$, $N_{TB,B}$ and N_U are separated by N_B. The boundary scenario, *i.e.* $\chi = 180°$, is solely represented by a phase sequence involving the isotropic phase and non-modulated nematics: $I \leftrightarrow N_U \leftrightarrow N_B$.

Increasing λ incrementally (Fig. 6b–e) leads to shrinkage of the stability regions for N_U and N_{TB} at the price of expanding the areas of N_B and $N_{TB,B}$. A climax is reached at the so-called "self-dual point" ($\lambda = 1/\sqrt{6}$) where exclusively N_B and $N_{TB,B}$ are present. Similarly to the phase diagram in Fig. 6a, three sets of phase sequences are achievable: $I \leftrightarrow N_{TB,B}$ ($\chi \in [90°,138°]$), $I \leftrightarrow N_B \leftrightarrow N_{TB,B}$ ($\chi \in (138°,180°)$), and $I \leftrightarrow N_B$ ($\chi = 180°$), with the difference that uniaxial phases are replaced by their biaxial counterparts. The evolution of θ, p and $w(\bar{\mathbf{Q}}(R_A))$ as a function of χ alongside the increase in magnitude of λ is also prominent (Fig. 6b–e). In particular, it applies to the behavior of $w(\bar{\mathbf{Q}}(R_A))$, which indicates that the biaxial nature of $N_{TB,B}$ intensifies in parallel with increasing λ, and at the self-dual point in the range of χ from 90° to 120° it switches sign and attains 0 (maximal biaxiality) at $\chi = 90°$ (see inset of Fig. 6e).

Our results are in line with experimental data,[8] which means that the postulate about the stability of the twist-bend nematic phase being governed by the molecule's bend angle is legitimate and crucial. Mandle *et al.*[8] examined a family of

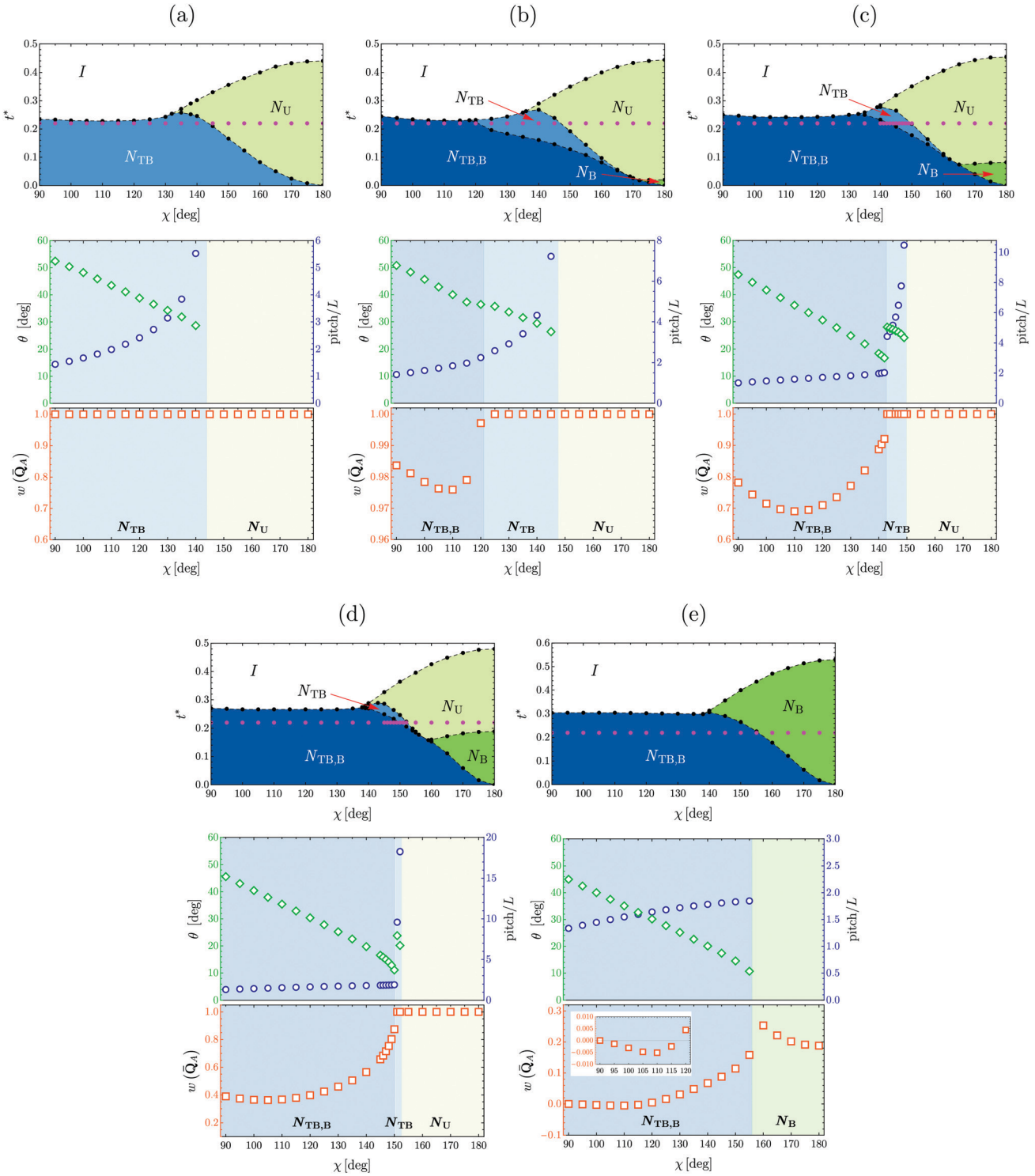

Fig. 6 Panel illustrating five phase diagrams in the domain of $\{\chi,t^*\}$ for a representative set of λ: 0 (a), 0.1 (b), 0.2 (c), 0.3 (d) and $1/\sqrt{6}$ (e). Below each phase diagram are two plots depicting the behavior of pitch, tilt angle (θ) and $w(\bar{\mathbf{Q}}(R_A)) \equiv w(\bar{\mathbf{Q}}_A)$ (eqn (8) and (10)) as a function of the bend angle χ for the respective points on the main phase diagram (purple points at $t^* = 0.22$). Inset in the bottom plot of (e) delineates the magnification of this plot in the range $\chi \in [90^\circ,120^\circ]$ and $w(\bar{\mathbf{Q}}(R_A)) \in [-0.01,0.01]$.

cyanobiphenyl dimers with varying linking groups and stated that the twist-bend nematic is thermally stable when χ is between 110° and 130°. Further increasing χ leads to the destabilization of N_{TB}.

Within the mean-field approach, we have investigated in detail two additional phase diagrams, with respect to our previous work,[27] for bent-core molecules with bend angles equal to 150° and 160°. It was possible to qualitatively identify

new phase transitions, namely: I $\leftrightarrow$ N_U $\leftrightarrow$ $N_{TB,B}$, and a straightforward transition between all phases anticipated by the mean-field model, *i.e.* I $\leftrightarrow$ N_U $\leftrightarrow$ N_B $\leftrightarrow$ N_{TB} $\leftrightarrow$ $N_{TB,B}$. Moreover, within the broad spectrum of bend angles we have shown how the interplay between χ and λ affects both the structural features and the mutual stability of nematic phases.

Conflicts of interest

There are no conflicts to declare.

Acknowledgements

This work was supported by Grant No. DEC-2013/11/B/ST3/04247 of the National Science Centre in Poland. W. T. acknowledges partial support by Marian Smoluchowski Scholarship (KNOW/58/SS/WT/2016) from Marian Smoluchowski Cracow Scientific Consortium ''Matter-Energy-Future'' within the KNOW grant and by Jagiellonian Interdisciplinary PhD Programme co-financed from the European Union funds under the European Social Fund (POWR.03.05.00-00-Z309/17-00).

Notes and references

1 A. Jákli, O. D. Lavrentovich and J. V. Selinger, *Rev. Mod. Phys.*, 2018, **90**, 045004.
2 R. B. Meyer, *Proceedings of the Les Houches Summer School on Theoretical Physics*, 1973, session No. XXV, New York, Gordon and Breach, 1976.
3 I. Dozov, *Europhys. Lett.*, 2001, **56**, 247.
4 M. Cestari, S. Diez-Berart, D. A. Dunmur, A. Ferrarini, M. R. de la Fuente, D. J. B. Jackson, D. O. Lopez, G. R. Luckhurst, M. A. Perez-Jubindo, R. M. Richardson, J. Salud, B. A. Timimi and H. Zimmermann, *Phys. Rev. E: Stat., Nonlinear, Soft Matter Phys.*, 2011, **84**, 031704.
5 D. Chen, J. H. Porada, J. B. Hooper, A. Klittnick, Y. Shen, M. R. Tuchband, E. Korblova, D. Bedrov, D. M. Walba, M. A. Glaser, J. E. Maclennan and N. A. Clark, *Proc. Natl. Acad. Sci. U. S. A.*, 2013, **110**, 15931.
6 V. Borshch, Y.-K. Kim, J. Xiang, M. Gao, A. Jákli, V. P. Panov, J. K. Vij, C. T. Imrie, M. G. Tamba, G. H. Mehl and O. D. Lavrentovich, *Nat. Commun.*, 2013, **4**, 2635.
7 D. A. Paterson, J. P. Abberley, W. T. Harrison, J. M. Storey and C. T. Imrie, *Liq. Cryst.*, 2017, **44**, 127.
8 R. J. Mandle, C. T. Archbold, J. P. Sarju, J. L. Andrews and J. W. Goodby, *Sci. Rep.*, 2016, **6**, 36682.
9 C. T. Archbold, R. J. Mandle, J. L. Andrews, S. J. Cowling and J. W. Goodby, *Liq. Cryst.*, 2017, **44**, 2079.
10 J. W. Goodby, *Liq. Cryst.*, 2017, **44**, 1755.
11 R. J. Mandle, *Chem. – Eur. J.*, 2017, **23**, 8771.
12 A. Lesac, U. Baumeister, I. Dokli, Z. Hameršak, T. Ivšić, D. Kontrec, M. Viskić, A. Knežević and R. J. Mandle, *Liq. Cryst.*, 2018, **45**, 1101.
13 E. E. Pocock, R. J. Mandle and J. W. Goodby, *Soft Matter*, 2018, **14**, 2508.
14 E. Cruickshank, M. Salamończyk, D. Pociecha, G. J. Strachan, J. M. D. Storey, C. Wang, J. Feng, C. Zhu, E. Gorecka and C. T. Imrie, *Liq. Cryst.*, 2019, **46**, 1595.
15 Y. Wang, G. Singh, D. M. Agra-Kooijman, M. Gao, H. K. Bisoyi, C. Xue, M. R. Fisch, S. Kumar and Q. Li, *CrystEngComm*, 2015, **17**, 2778.
16 S. M. Jansze, A. Martínez-Felipe, J. M. D. Storey, A. T. M. Marcelis and C. T. Imrie, *Angew. Chem., Int. Ed.*, 2015, **54**, 643.
17 R. J. Mandle and J. W. Goodby, *Angew. Chem., Int. Ed.*, 2018, **57**, 7096.
18 R. J. Mandle and J. W. Goodby, *RSC Adv.*, 2016, **6**, 34885.
19 R. J. Mandle, *Soft Matter*, 2016, **12**, 7883.
20 W. D. Stevenson, J. An, X.-B. Zeng, M. Xue, H.-x. Zou, Y.-s. Liu and G. Ungar, *Soft Matter*, 2018, **14**, 3003.
21 J. P. Abberley, R. Killah, R. Walker, J. M. D. Storey, C. T. Imrie, M. Salamończyk, C. Zhu, E. Górecka and D. Pociecha, *Nat. Commun.*, 2018, **9**, 228.
22 M. T. Murachver, A. Nemati, M. Salamończyk, C. Bullock, Z. Sabata, H. Rahmani, T. Vorobiova, A. Izadnegahdar, S. M. Salili, V. Norman, C. Zhu, T. Hegmann, S. N. Sprunt, J. T. Gleeson and A. I. Jákli, *Soft Matter*, 2019, **15**, 3283.
23 R. Walker, D. Pociecha, G. J. Strachan, J. M. D. Storey, E. Górecka and C. T. Imrie, *Soft Matter*, 2019, **15**, 3188.
24 Y. Arakawa, K. Komatsu and H. Tsuji, *New J. Chem.*, 2019, **43**, 6786.
25 Y. Arakawa and H. Tsuji, *J. Mol. Liq.*, 2019, **289**, 111097.
26 J. P. Abberley, J. M. D. Storey and C. T. Imrie, *Liq. Cryst.*, 2019, **46**, 2102.
27 W. Tomczyk, G. Pająk and L. Longa, *Soft Matter*, 2016, **12**, 7445.
28 R. Rosso, *Liq. Cryst.*, 2007, **34**, 737.
29 T. B. T. To, T. J. Sluckin and G. R. Luckhurst, *Liq. Cryst.*, 2016, **43**, 1448.
30 A. Ferrarini, *Liq. Cryst.*, 2017, **44**, 45.
31 L. Longa and G. Pająk, *Liq. Cryst.*, 2005, **32**, 1409.
32 L. Longa, P. Grzybowski and S. Romano, *et al.*, *Phys. Rev. E: Stat., Nonlinear, Soft Matter Phys.*, 2005, **71**, 051714.
33 D. Allender and L. Longa, *Phys. Rev. E: Stat., Nonlinear, Soft Matter Phys.*, 2008, **78**, 011704.
34 P. G. de Gennes and J. Prost, *The Physics of Liquid Crystals*, Clarendon Press, 2nd edn, 1993.
35 M. Osipov and G. Pająk, *Phys. Rev. E: Stat., Nonlinear, Soft Matter Phys.*, 2012, **85**, 21701.
36 G. Pająk and M. A. Osipov, *Phys. Rev. E: Stat., Nonlinear, Soft Matter Phys.*, 2013, **88**, 12507.
37 C. Greco, G. R. Luckhurst and A. Ferrarini, *Soft Matter*, 2014, **10**, 9318.
38 T. B. T. To, T. J. Sluckin and G. R. Luckhurst, *Phys. Chem. Chem. Phys.*, 2017, **19**, 29321.
39 S. Kumar and S. K. Pal, *Liquid Crystal Dimers*, Cambridge University Press, 2017.
40 A. A. Dawood, M. C. Grossel, G. R. Luckhurst, R. M. Richardson, B. A. Timimi, N. J. Wells and Y. Z. Yousif, *Liq. Cryst.*, 2016, **43**, 2.

41 A. A. Dawood, M. C. Grossel, G. R. Luckhurst, R. M. Richardson, B. A. Timimi, N. J. Wells and Y. Z. Yousif, *Liq. Cryst.*, 2017, **44**, 106.
42 C. T. Archbold, E. J. Davis, R. J. Mandle, S. J. Cowling and J. W. Goodby, *Soft Matter*, 2015, **11**, 7547.
43 N. Boccara, R. Mejdani and L. De Seze, *J. Phys. France*, 1977, **38**, 149.
44 F. Biscarini, C. Chiccoli, P. Pasini, F. Semeria and C. Zannoni, *Phys. Rev. Lett.*, 1995, **75**, 1803.